Composite Structures 174 (2017) 70–86

Contents lists available at ScienceDirect

Composite Structures

journal homepage: www.elsevier.com/locate/compstruct

Bending behaviour of two directional functionally graded sandwich beams by using a quasi-3d shear deformation theory

Armağan Karamanlı

Department of Mechatronics, Faculty of Engineering and Architecture, Istanbul Gelişim University, 34215 Istanbul, Turkey

ARTICLE INFO

Article history:
Received 9 February 2017
Revised 4 April 2017
Accepted 18 April 2017
Available online 21 April 2017

Keywords:
Meshless method
Functionally graded sandwich beam
Strecthing effect
SSPH method
Quasi-3D shear deformation theory

ABSTRACT

This paper presents the static behaviour of two-directional functionally graded (FG) sandwich beams subjected to various sets of boundary conditions by using a quasi-3D shear deformation theory and the Symmetric Smoothed Particle Hydrodynamics (SSPH) method. The SSPH code, which is developed based on the present formulation of the FG sandwich beam, is validated by solving a simply supported conventional functionally graded beam problem. Numerical results which are in terms of maximum dimensionless transverse deflections, dimensionless axial, normal and shear stresses are compared with the analytical solutions and the results from previous studies. Various FG sandwich beam structures are investigated by considering different aspect ratios (L/h) and sets of boundary conditions and using power-law distribution.

© 2017 Elsevier Ltd. All rights reserved.

1. Introduction

In recent years, the use of the structures which are made of functionally graded materials have been increasing in many modern engineering applications such as aerospace, marine, automotive, nuclear energy, biomedical and civil engineering due to varying material properties over a changing dimension which allow to enhance the bond strength through the layer interfaces, high resistance to temperature shocks, lower transverse shear stresses and high strength to weight ratio.

Due to the significant shear deformation effects especially for the thick FGBs, three main theories that are first-order shear deformation theory, higher-order shear deformation theory and quasi-3D shear deformation theory have been employed by the researchers to predict and understand the static, vibration and buckling responses of these structures during the last decade [1–36].

On the other hand, a new type functionally graded material (FGM) with material properties varying in two or three directions is needed to fulfill the technical requirements such as the temperature and stress distributions in two or three directions for aerospace craft and shuttles where the conventional FGMs (or 1D-FGM) with material properties which vary in one direction are not so efficient [37]. The mechanical and thermal behaviour of two-directional FG structures have been investigated so far. The 2D steady-state free and forced vibrations of two-directional FGBs by using the Element Free Galerkin Method are analyzed in [38]. The state-space based differential quadrature method is employed to obtain the semi-analytical elasticity solutions for bending and thermal deformations of functionally graded beams (FGBs) with various end conditions [39]. A symplectic elasticity solution for static and free vibration analyses of two-directional FGBs with the material properties varying exponentially in both axial and thickness directions are presented in [40]. The buckling behaviour of Timoshenko beams composed of two directional FGM is studied in [41]. The static behaviour of the two directional FGBs by using various beam theories is presented in [42]. The flexure of the two directional FG curved beams is analyzed in [43].

As it is seen from above discussions, the studies related to static and dynamic analysis of the two-directional FGBs are very limited. Moreover, there is no work available in the literature related to the elastostatic analysis of the two-directional FG sandwich beams by employing a quasi-3D theory which includes both shear deformation and thickness stretching effects according to the author knowledge. Since the thickness-stretching effect becomes very important especially for the thick two directional FG sandwich beams, a quasi-3D theory should be considered for this complicated problem. One may easily show that the numerical methods such as finite element methods (FEM), meshless methods, generalized differential quadrature method (GDQM), etc. can be used to overcome these problems which have complex governing equations.

Meshless methods are the most promising and have attracted considerable attention for the analysis of engineering problems with intrinsic complexity. Meshless methods are widely used in

E-mail address: armagan_k@yahoo.com

http://dx.doi.org/10.1016/j.compstruct.2017.04.046
0263-8223/© 2017 Elsevier Ltd. All rights reserved.

static and dynamic analyses of the isotropic, laminated composite and FGBs problems [44–50]. However, the studies are very limited regarding to the analysis of two directional FG structures by employing a meshless method [38,42,51–53].

The main novelty of this paper is that the elastostatic behaviour of the two directional FG sandwich beams are analyzed based on a quasi-3D theory by using the SSPH method for the first time. The SSPH codes are developed to determine the displacement and stresses of two-directional FG sandwich beams for various boundary conditions, power-law indexes and sandwich structures. Numerical results are compared with the analytical solutions and the results from previous studies.

In Section 2, the formulation of the basis function of the SSPH method is given. In Section 3, the homogenization of material properties of the two directional FG sandwich beam is presented. The formulation of the quasi-3D theory is given in Section 4. In Section 5, numerical results are given for the problems with three different boundary conditions which are simply supported (SS), clamped-clamped (CC) and clamped-free (CF).

2. Formulation of symmetric smoothed particle hydrodynamics method

Taylor Series Expansion (TSE) of a scalar function for 1D case can be given by

$$f(\xi) = f(x) + (\xi - x)f'(x) + \frac{1}{2!}(\xi - x)^2 f''(x) + \frac{1}{3!}(\xi - x)^3 f'''(x) + \frac{1}{4!}(\xi - x)^4 f^{(IV)}(x) + \frac{1}{5!}(\xi - x)^5 f^{(V)}(x) + \frac{1}{6!}(\xi - x)^6 f^{(VI)}(x) + \cdots \quad (1)$$

where $f(\xi)$ is the value of the function at ξ located in near of x. If the zeroth to sixth order terms are employed and the higher order terms are neglected, the Eq. (1) can be written as

$$f(\xi) = \boldsymbol{P}(\xi, x)\boldsymbol{Q}(x) \quad (2)$$

where

$$\boldsymbol{Q}(x) = \left[f(x), \frac{df(x)}{dx}, \frac{1}{2!}\frac{d^2 f(x)}{dx^2}, \ldots, \frac{1}{6!}\frac{d^6 f(x)}{dx^6} \right]^T \quad (3)$$

$$\boldsymbol{P}(\xi, x) = [1, (\xi - x), (\xi - x)^2, \ldots, (\xi - x)^6] \quad (4)$$

The number of terms employed in the TSE can be increased to improve the accuracy depending on the order of the governing equations. However, increasing the number of terms to be employed definitely increases the CPU time and may decrease the effectiveness of the method. Determination of the number of terms mainly depends on the experience of the researcher. To determine the unknown variables given in the matrix $\mathbf{Q}(x)$, both sides of Eq. (2) are multiplied with $W(\xi, x)\mathbf{P}(\xi, x)^T$ and evaluated for every node in the CSD. In the global numbering system, let the particle number of the jth particle in the compact support of $W(\xi, x)$ be r (j). The following equation is obtained

$$\sum_{j=1}^{N(x)} f(\xi^{r(j)}) W(\xi^{r(j)}, x)\boldsymbol{P}(\xi^{r(j)}, x)^T = \sum_{j=1}^{N(x)} [\boldsymbol{P}(\xi^{r(j)}, x)^T W(\xi^{r(j)}, x)\boldsymbol{P}(\xi^{r(j)}, x)]\boldsymbol{Q}(x) \quad (5)$$

where N(x) is the number nodes in the compact support domain (CSD) of the $W(\xi, x)$ as shown in Fig. 1.

Then, Eq. (5) can be given by

$$\boldsymbol{C}(\xi, x)\boldsymbol{Q}(x) = \boldsymbol{D}(\xi, x)\boldsymbol{F}^{(x)}(\xi, x) \quad (6)$$

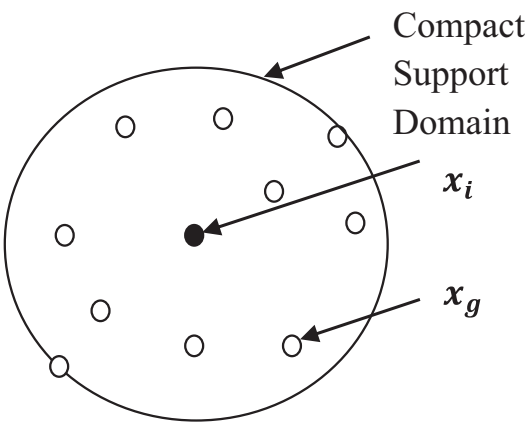

Fig. 1. Compact support of the weight function $W(\xi, x)$ for the node located at $x = (x_i, y_i)$.

where $\mathbf{C}(\xi, x) = \mathbf{P}(\xi, x)^T \mathbf{W}(\xi, x)\mathbf{P}(\xi, x)$ and $\mathbf{D}(\xi, x) = \mathbf{P}(\xi, x)^T \mathbf{W}(\xi, x)$.

The solution of Eq. (6) is given by

$$\boldsymbol{Q}(x) = \boldsymbol{K}(\xi, x)\boldsymbol{F}(\xi) \quad (7)$$

where $\mathbf{K}^{(x)}(\xi, x) = \mathbf{C}(\xi, x)^{-1}\mathbf{D}(\xi, x)$. Eq. (7) can be also written as follows

$$Q_I(x) = \sum_{J=1}^{M} K_{IJ} F_J, \quad I = 1, 2, \ldots, 7 \quad (8)$$

where M is the number of nodes and $F_j = f(\xi^J)$. Seven components of Eq. (8) for 1D case are written as

$$\begin{aligned}
f(x) &= Q_1(x) = \sum_{J=1}^{M} K_{1J} F_J \\
\tfrac{df(x)}{dx} &= Q_2(x) = \sum_{J=1}^{M} K_{2J} F_J \\
\tfrac{d^2 f(x)}{dx^2} &= 2! Q_3(x) = 2! \sum_{J=1}^{M} K_{3J} F_J \\
\tfrac{d^3 f(x)}{dx^3} &= 3! Q_4(x) = 3! \sum_{J=1}^{M} K_{4J} F_J \\
\tfrac{d^4 f(x)}{dx^4} &= 4! Q_5(x) = 4! \sum_{J=1}^{M} K_{5J} F_J \\
\tfrac{d^5 f(x)}{dx^5} &= 5! Q_6(x) = 5! \sum_{J=1}^{M} K_{6J} F_J \\
\tfrac{d^6 f(x)}{dx^6} &= 6! Q_7(x) = 6! \sum_{J=1}^{M} K_{7J} F_J
\end{aligned} \quad (9)$$

Details of the SSPH method can be found in [42,54–57].

3. Homogenization of material properties

Consider a two-directional functionally graded beam namely Type A as shown in Fig 2a, which is made of a mixture of ceramic and metal, with length L, width b and thickness h. Two types of FG sandwich beams namely 2D-FG and Ceramic Faces and 1D-FG Core (Type B) and 2D-FG faces ceramic core (Type C) are considered.

The rule of mixture is used to find the effective material properties at a point. According to the rule of mixtures, the effective material properties of the beam such as Young's modulus E and shear modulus G can be given by

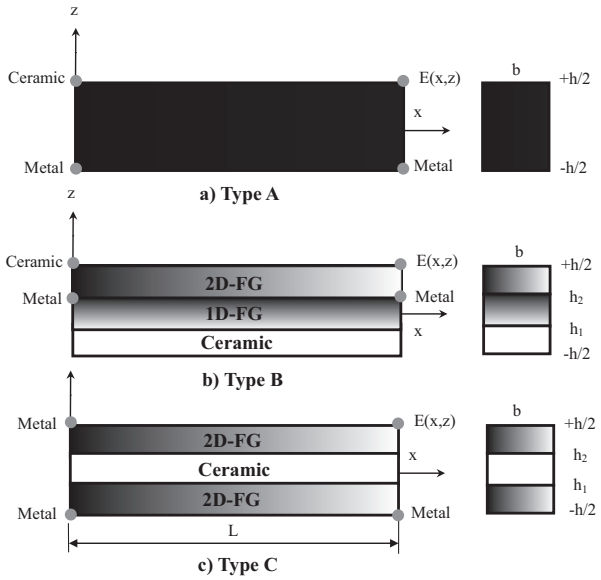

Fig. 2. Geometry and coordinate of a two-directional FG Sandwich Beams.

$$E(x,z) = E_1V_1(x,z) + E_2V_2(x,z)$$
$$G(x,z) = G_1V_1(x,z) + G_2V_2(x,z) \tag{10}$$

where E_1, E_2, G_1 and G_2 are the material properties of two constituents, V_1 and V_2 are the volume fractions of the constituents. The relation between the volume fractions can be expressed as follows;

$$V_1(x,z) + V_2(x,z) = 1 \tag{11}$$

3.1. Type A: 2D-FG Beam

According to the power-law rule, the volume fraction of the ceramic can be given by

$$V_c(x,z) = \left(1 - \frac{x}{2L}\right)^{p_x}\left(\frac{1}{2} + \frac{z}{h}\right)^{p_z} \tag{12}$$

where p_x and p_z are the gradation exponents (power-law index) which determine the material properties through the thickness (h) and length of the beam (L). When the p_x and p_z are set to zero, the beam becomes homogeneous. The effective material properties can be found by using the Eqs. (10)–(12) as follows

$$E(x,z) = (E_c - E_m)\left(1 - \tfrac{x}{2L}\right)^{p_x}\left(\tfrac{1}{2} + \tfrac{z}{h}\right)^{p_z} + E_m$$
$$G(x,z) = (G_c - G_m)\left(1 - \tfrac{x}{2L}\right)^{p_x}\left(\tfrac{1}{2} + \tfrac{z}{h}\right)^{p_z} + G_m \tag{13}$$

3.2. Type B: Sandwich Beam with 2D-FG and Ceramic Faces and 1D-FG Core

The upper face of the sandwich beam is made of 2D-FG, the lower face is made of ceramic and the core is made of 1D-FG as shown in Fig. 2b. The volume fraction of the ceramic phase $V_c^{(i)}$ given by;

$$V_c^{(1)} = \left(1 - \tfrac{x}{2L}\right)^{p_x}\left(\tfrac{2(z-h_2)}{h-2h_2}\right)^{p_z} \quad for z \in [h_2, h/2]$$
$$V_c^{(2)} = \left(\tfrac{z-h_2}{h_1-h_2}\right)^{p_z} \quad for z \in [h_1, h_2] \tag{14}$$
$$V_c^{(3)} = 1 \quad for z \in \left[h_1, -\tfrac{h}{2}\right]$$

3.3. Type C: Sandwich Beam with 2D-FG Faces and Ceramic Core

The two faces of the sandwich beam are made of 2D-FG and the core is made of ceramic as shown in Fig. 2c. The volume fraction of the metal phase $V_m^{(i)}$ given by;

$$V_m^{(1)} = \left(1 - \tfrac{x}{2L}\right)^{p_x}\left(\tfrac{2(z-h_2)}{h-2h_2}\right)^{p_z} \quad for z \in [h_2, h/2]$$
$$V_m^{(2)} = 0 \quad for z \in [h_1, h_2] \tag{15}$$
$$V_m^{(3)} = \left(1 - \tfrac{x}{2L}\right)^{p_x}\left(\tfrac{2(h_1-z)}{h+2h_1}\right)^{p_z} \quad for z \in [h_1, -h/2]$$

4. Mathematical formulation

The axial and transverse displacements of a beam by using the present quasi-3D theory [28] including both shear deformation and thickness stretching effects are given by

$$\begin{aligned} U(x,z) &= u(x,t) - z\tfrac{dw_b(x)}{dx} - \tfrac{4z^3}{3h^2}\tfrac{dw_s(x)}{dx} \\ &= u(x) - zw_b'(x) - f(z)w_s' \end{aligned} \tag{16a}$$

$$\begin{aligned} W(x,z) &= w_b(x) + w_s(x) + (1 - \tfrac{4z^2}{h^2})w_z(x) \\ &= w_b(x) + w_s(x) + g(z)w_z \end{aligned} \tag{16b}$$

where u, w_b, w_s and w_z are four unknowns to be determined. The only nonzero strains associated with the displacement field given in Eq. (16) can be written by:

$$\varepsilon_x = \frac{\partial U}{\partial x} = u' - zw_b'' - f(z)w_s'' \tag{17a}$$

$$\varepsilon_z = \frac{\partial W}{\partial z} = g'(z)w_z \tag{17b}$$

$$\gamma_{xz} = \frac{\partial W}{\partial x} + \frac{\partial U}{\partial z} = g(z)(w_b' + w_s') \tag{17c}$$

The following linear elastic constitutive equation can be written by using the related stresses and strains:

$$\begin{bmatrix}\sigma_x \\ \sigma_z \\ \sigma_{xz}\end{bmatrix} = \frac{E(x,z)}{1-\nu^2}\begin{bmatrix}1 & \nu & 0 \\ \nu & 1 & 0 \\ 0 & 0 & \frac{1-\nu}{2}\end{bmatrix}\begin{bmatrix}\varepsilon_x \\ \varepsilon_z \\ \gamma_{xz}\end{bmatrix} \tag{18a}$$

$$\begin{bmatrix}\sigma_x \\ \sigma_z \\ \sigma_{xz}\end{bmatrix} = \frac{E(x,z)}{1-\nu^2}\begin{bmatrix}u' - zw_b'' - fw_s'' + \nu g'w_z \\ \nu u' - \nu zw_b'' - \nu fw_s'' + g'w_z \\ (\frac{1-\nu}{2})g(w_b' + w_s')\end{bmatrix} \tag{18b}$$

To obtain the governing equations, the virtual strain energy of the beam can be written by:

$$\delta U = \int_0^L \int_A (\sigma_x\delta\varepsilon_x + \sigma_{xz}\delta\gamma_{xz} + \sigma_z g'\delta\varepsilon_z)dAdx \tag{19}$$

The stress resultants $N_x, M_x^b, M_x^s, Q_{xz}$ and R_z can be written respectively as follows:

$$N_x = \int_{-h/2}^{+h/2} b\sigma_x dz \tag{20a}$$

$$M_x^b = \int_{-h/2}^{+h/2} b\sigma_x z dz \tag{20b}$$

$$M_x^s = \int_{-h/2}^{+h/2} b\sigma_x f dz \tag{20c}$$

$$Q_{xz} = \int_{-h/2}^{+h/2} b\sigma_{xz} g dz \tag{20d}$$

$$R_z = \int_{-h/2}^{+h/2} b\sigma_z g' dz \tag{20e}$$

By using the Eq. (20), one can rewrite the Eq. (18) as:

$$\delta U = \int_0^L [N_x \delta u' - M_x^b \delta w_b'' - M_x^s \delta w_s'' + Q_{xz}(\delta w_s' + \delta w_z') + R_z \delta w_z] dx \tag{21}$$

The virtual potential energy of the transverse load $q(x)$ is given by

$$\delta V = -\int_0^L q(\delta w_b + \delta w_s) dx \tag{22}$$

Since the total virtual work done equals zero and the coefficients of $\delta u, \delta w_b, \delta w_s$ and δw_z are zero in $0 < x < L$, one can obtain the following governing equations,

$$\frac{dN_x}{dx} = 0 \tag{23a}$$

$$\frac{d^2 M_x^b}{dx^2} + q(x) = 0 \tag{23b}$$

$$\frac{d^2 M_x^s}{dx^2} + \frac{dQ_{xz}}{dx} + q(x) = 0 \tag{23c}$$

$$\frac{dQ_{xz}}{dx} - R_z = 0 \tag{23d}$$

By using Eq. (18), the stress resultants given in Eq. (20) can be expressed as,

$$\begin{Bmatrix} N_x \\ M_x^b \\ M_x^s \\ Q_{xz} \\ R_z \end{Bmatrix} = \begin{bmatrix} A & B & B_s & X & 0 \\ B & D & D_s & Y & 0 \\ B_s & D_s & H & Y_s & 0 \\ X & Y & Y_s & Z & 0 \\ 0 & 0 & 0 & 0 & A_s \end{bmatrix} \begin{Bmatrix} u' \\ -w_b'' \\ -w_s'' \\ w_z \\ w_s' + w_z' \end{Bmatrix} \tag{24}$$

where

$$(A, B, B_s, D, D_s, H, Z) = \int_{-h/2}^{+h/2} \frac{E(x,z) b}{1-\nu^2} (1, z, f, z^2, fz, f^2, g'^2) dz \tag{25a}$$

$$A_s = \int_{-h/2}^{+h/2} \frac{E(x,z) b}{2(1+\nu)} g^2 dz \tag{25b}$$

$$(X, Y, Y_s) = \int_{-h/2}^{+h/2} \frac{E(x,z) \nu b}{1-\nu^2} g'(1, z, f) dz \tag{25c}$$

The governing equations of the quasi-3D theory can be obtained by substituting Eq. (24) into Eq. (23) as:

$$Au'' + A'u' - (Bw_b''' + B'w_b'') - (B_s w_s''' + B_s' w_s'') + Xw_z' + X'w_z = 0 \tag{26a}$$

$$Bu''' + 2B'u'' + B''u' - (Dw_b^{(IV)} + 2D'w_b''' + D''w_b'') - (D_s w_s^{(IV)} + 2D_s' w_s''' + D_s'' w_s'') + Yw_z'' + 2Y'w_z' + Y''w_z + q = 0 \tag{26b}$$

$$B_s u''' + 2B_s' u'' + B_s'' u' - (D_s w_b^{(IV)} + 2D_s' w_b''' + D_s'' w_b'') - (Hw_s^{(IV)} + 2H'w_s''' + H''w_s'') + Y_s w_z'' + 2Y_s' w_z' + Y_s'' w_z + A_s(w_s'' + w_z'') + A_s'(w_s' + w_z') + q = 0 \tag{26c}$$

$$-Xu' + Yw_b'' + Y_s w_s'' + A_s(w_s'' + w_z'') + A_s'(w_s' + w_z') - Zw_z = 0 \tag{26d}$$

The natural boundary conditions are of the form:

$$\delta u : N_x \tag{27a}$$

$$\delta w_b : M_x^{b'} \tag{27b}$$

$$\delta w_b' : M_x^b \tag{27c}$$

$$\delta w_s : M_x^{s'} + Q_{xz} \tag{27d}$$

$$\delta w_s' : M_x^s \tag{27e}$$

$$\delta w_z : Q_{xz} \tag{27f}$$

4.1. Representation of the governing equations by using the SSPH method

The governing equations of the problem based on the present quasi-3D beam theory can be written in a similar way by replacing $f(x)$ given in Eq. (9) with $u(x), w_b(x), w_s(x)$ and $w_z(x)$ as follows,

$$\sum_{J=1}^{M} [2AK_{2J} + A'K_{1J}] u_j - \sum_{J=1}^{M} [6BK_{4J} + 2B'K_{3J}] w_{b_j} - \sum_{J=1}^{M} [6B_s K_{4J} + 2B_s' K_{3J}] w_{s_j} + \sum_{J=1}^{M} [XK_{2J} + X'K_{1J}] w_{z_j} = 0 \tag{28a}$$

$$\sum_{J=1}^{M} [6BK_{4J} + 4B'K_{3J} + B''K_{2J}] u_j - \sum_{J=1}^{M} [24DK_{5J} + 12D'K_{4J} + 2D''K_{3J}] w_{b_j} - \sum_{J=1}^{M} [24D_s K_{5J} + 12D_s' K_{4J} + 2D_s'' K_{3J}] w_{s_j} + \sum_{J=1}^{M} [2YK_{3J} + 2Y'K_{2J} + Y''K_{1J}] w_{z_j} = -q \tag{28b}$$

$$-\sum_{J=1}^{M} XK_{2J} u_j + \sum_{J=1}^{M} 2YK_{3J} w_{b_j} + \sum_{J=1}^{M} [2Y_s K_{3J} + 2A_s K_{3J} + A_s' K_{2J}] w_{s_j} + \sum_{J=1}^{M} [2A_s K_{3J} + A_s' K_{2J} - ZK_{1J}] w_{z_j} = 0 \tag{28c}$$

$$\sum_{J=1}^{M} [6B_s K_{4J} + 4B_s' K_{3J} + B_s'' K_{2J}] u_j - \sum_{J=1}^{M} [24D_s K_{5J} + 12D_s' K_{4J} + 2D_s'' K_{3J}] w_{b_j} - \sum_{J=1}^{M} [24HK_{5J} + 12H'K_{4J} + 2H''K_{3J} - 2A_s K_{3J} - A_s' K_{2J}] w_{s_j} + \sum_{J=1}^{M} [2Y_s K_{3J} + 2Y_s' K_{2J} + Y_s'' K_{1J} + 2A_s K_{3J} + A_s' K_{2J}] w_{z_j} = -q \tag{28d}$$

5. Numerical results

The bending behaviour of the two directional FG sandwich beams is investigated by using a quasi-3D shear deformation theory. The numerical results are obtained by using the SSPH method for various gradation exponents, aspect ratios and sets of boundary conditions. Since there is no available previous results based on a higher order shear deformation theory and a quasi-3D shear deformation theory for the bending analysis of two-directional FGBs with power law rule, the developed SSPH code is verified by solving a simply supported conventional FGB problem subjected

to uniformly distributed load. The numerical solutions are compared with the solutions from previous studies along with the analytical solutions [27,28]. The dimensionless maximum transverse deflections, axial, normal and shear stresses are calculated to make the comparisons on a fair ground.

For each problem studied here, the physical parameters of the beam are L = 2 m and b = 0.1 m. Two different two aspect ratios, L/h = 5 and 20 are considered for the boundary conditions defined as S-S and C-C. The numerical solutions could not be obtained for the aspect ratio (L/h) which is greater than 5 for the boundary condition defined as CF. The possible reasons behind this case are discussed in section 5.2.3. The distributed load q_0 is set to 10,000 N/m. The material properties of the two constitutes are given by

$$Ceramic\ (Al_2O_3):\ E_1 = 380\ \text{GPa}\ and\ \nu_1 = 0.3$$

$$Metal\ (Aluminium):\ E_2 = 70\ \text{GPa}\ and\ \nu_2 = 0.3$$

The following non-dimensional quantities are used for the representation of the results;

Non-dimensional transverse deflection of the beam:

$$\begin{aligned}\overline{w} &= \frac{100E_2bh^3}{q_0L^4}W(x,0)\ for\ SS\ and\ CC\ beams\\ \overline{w} &= \frac{100E_2bh^3}{q_0L^4}W(L,0)\ for\ CF\ beam\end{aligned} \tag{29}$$

Non-dimensional axial, normal and shear stresses of the beam:

$$\begin{aligned}\overline{\sigma}_x &= \frac{bh}{q_0L}\sigma_x\left(\frac{L}{2},z\right)\\ \overline{\sigma}_z &= \frac{bh}{q_0L}\sigma_z\left(\frac{L}{2},z\right)\\ \overline{\sigma}_{xz} &= \frac{h}{q_0L}\sigma_{xz}(0,z)\end{aligned} \tag{30}$$

5.1. Verification and comparison studies

To verify the developed code, a simply supported FGB under uniformly distributed load is considered. Since the SSPH method is employed to solve an engineering problem with more than 2 unknowns for the first time, the detailed analysis is required. After performing comprehensive analysis with the weight functions employed by the researchers in [42,54–57], satisfactory results could not be obtained. Moreover, the weight functions given in [58] except the one given in Eq. (31) also could not provide satisfactory results. Therefore, the following weight function proposed in [58] is employed for the analysis studied within this paper,

$$W(x,\xi) = \begin{cases} \left(1-\frac{d}{\rho}\right)^7 35\left(\frac{d}{\rho}\right)^6 + 245\left(\frac{d}{\rho}\right)^5 + 720\left(\frac{d}{\rho}\right)^4 + 1120\left(\frac{d}{\rho}\right)^3 & \\ \quad +928\left(\frac{d}{\rho}\right)^2 + 336\left(\frac{d}{\rho}\right) + 48 & 0 \leqslant d \leqslant \rho \\ 0 & d > \rho \end{cases} \tag{31}$$

where $d = |x-\xi|/h$, h is the smoothing length and ρ is the scaling factor that determines the size of the support domain. In Table 1, the results of the convergence studies are given. The dimensionless maximum transverse deflections of a FG beam under uniformly distributed load are calculated for different node distributions, smoothing lengths and end conditions, mainly SS and CC for $p_z = 0$, $p_x = 0$ and L/h = 5. The scaling factor is set to 8 as given in [42]. For the numerical calculations to be performed by the SSPH method for the convergence studies uniformly distributed 81, 161 and 201 nodes are considered. The SSPH method shows stability in terms of the computed transverse deflection values when

Table 1
Convergence studies of the developed SSPH code for S-S and C-C FGBs, L/h = 5.

Method		Theory	ε_z	SS	CC
				p = 0	p = 0
Vo et al. [28] Navier		Present	≠0	3.1397	0.8327
Number of nodes	Smoothing length				
81	1Δ	Present	≠0	3.1473	0.8968
	1.1Δ	Present	≠0	3.1354	0.8346
	1.2Δ	Present	≠0	3.0815	0.8372
	1.3Δ	Present	≠0	3.1408	0.8376
161	1Δ	Present	≠0	3.1468	0.8388
	1.1Δ	Present	≠0	3.1394	0.8348
	1.2Δ	Present	≠0	3.1152	0.8897
	1.3Δ	Present	≠0	3.1245	0.8350
201	1Δ	Present	≠0	3.1406	0.8341
	1.1Δ	Present	≠0	3.1402	0.8349
	1.2Δ	Present	≠0	3.1381	0.8372
	1.3Δ	Present	≠0	3.1425	0.8421

Table 2
Verification studies of the developed meshless code for S-S FGB, dimensionless maximum transverse deflections for various gradation exponents.

Method	Theory	ε_z	p = 0	p = 1	p = 2	p = 5	p = 10
L/h = 5							
Li et al. [27]	TBT	= 0	3.1657	6.2599	8.0602	9.7802	10.8979
Vo et al. [28] Navier	TBT	= 0	3.1654	6.2594	8.0677	9.8281	10.9381
	Present	≠0	3.1397	6.1338	7.8606	9.6037	10.7578
Vo et al. [28] FEM	TBT	= 0	3.1654	6.2590	8.0668	9.8271	10.9375
	Present	≠0	3.1397	6.1334	7.8598	9.6030	10.7572
SSPH	Present	≠0	3.1402	6.1343	7.8602	9.6041	10.7571
L/h = 20							
Li et al. [27]	TBT	= 0	2.8962	5.8049	7.4415	8.8151	9.6879
Vo et al. [28] Navier	TBT	= 0	2.8962	5.8049	7.4421	8.8182	9.6905
	Present	≠0	2.8947	5.7201	7.2805	8.6479	9.5749
Vo et al. [28] FEM	TBT	= 0	2.8963	5.8045	7.4412	8.8173	9.6899
	Present	≠0	2.8947 p = 0	5.7197	7.2797	8.6471	9.5743
SSPH	Present	≠0	2.8952	5.7215	7.2826	8.6485	9.5745

employing 201 nodes in the problem domain as the smoothing length varies. Therefore, for the analysis to be performed for SS and CC boundary conditions, the number of nodes is employed as 201, the radius of the support domain (ρ) is chosen as 8 and the smoothing length (h) which provides the most accurate results sets to 1.1Δ where Δ is the minimum distance between two adjacent nodes. Regarding to the analysis for the CF beam, the numerical calculations are performed according to the following meshless parameters which are found by performing the trial and error method; the number of nodes in the problem domain is employed as 247, the radius of the support domain (ρ) is chosen as 5.302 and the smoothing length (h) sets to 1.2Δ. A generic method to find good meshless parameters for the SSPH method is still to be found.

The maximum non-dimensional transverse deflections, axial, normal and shear stresses obtained based on the present quasi-3D shear deformation theory for various aspect ratios and gradation exponents in the z direction are given in Table 2–5 along with the results from previous studies and the analytical solution of the problem. It is clear that the results obtained by using the SSPH method agree completely with those of previous papers [27,28]. Table 2–5 show that the results obtained by the SSPH method are in excellent agreement with the results given in [27,28]. And finally, because of the stretching effect, the transverse deflections computed based on the quasi-3D theory are slightly smaller than those obtained from the Third Order Beam Theory (TBT). Due to this agreement, the verification of the developed code is established.

5.2. Elastostatic analysis of Two-Directional FGBs

Three different boundary conditions, S-S, C-C and C-F are considered respectively for the bending analysis of two directional FG sandwich beams subjected to uniformly distributed load. The transverse deflections, axial, normal and shear stresses are computed based on the present quasi-3D theory for various gradation exponents in both direction and aspect ratios. The details of the boundary conditions (BCs) used for the numerical analysis are given in Table 6.

Table 3
Verification studies of the developed meshless code for S-S FGB, dimensionless axial stress $\overline{\sigma}_x\left(\frac{L}{2},\frac{h}{2}\right)$ for various gradation exponents.

Method	Theory	ε_z		p = 1	p = 2	p = 5	p = 10
L/h = 5							
Li et al. [27]	TBT	= 0	3.8020	5.8837	6.8812	8.1030	9.7063
Vo et al. [28] Navier	TBT	= 0	3.8020	5.8836	6.8826	8.1106	9.7122
	Present	≠0	3.8005	5.8812	6.8818	8.1140	9.7164
Vo et al. [28] FEM	TBT	= 0	3.8040	5.8870	6.8860	8.1150	9.7170
	Present	≠0	3.8020	5.8840	6.8860	8.1190	9.7220
SSPH	Present	≠0	3.8005	5.8815	6.8821	8.1145	9.7170
L/h = 20							
Li et al. [27]	TBT	= 0	15.0130	23.2054	27.0989	31.8112	38.1372
Vo et al. [28] Navier	TBT	= 0	15.0129	23.2053	27.0991	31.8130	38.1385
	Present	≠0	15.0125	23.2046	27.0988	31.8137	38.1395
Vo et al. [28] FEM	TBT	= 0	15.0200	23.2200	27.1100	31.8300	38.1600
	Present	≠0	15.0200	23.2200	27.1100	31.8300	38.1600
SSPH	Present	≠0	15.0147	23.2099	27.1122	31.8070	38.1252

Table 4
Verification studies of the developed meshless code for S-S FGB, dimensionless transverse shear stress $\overline{\sigma}_{xz}(0,0)$ for various gradation exponents.

Method	Theory	ε_z	p = 0	p = 1	p = 2	p = 5	p = 10
L/h = 5							
Li et al. [27]	TBT	= 0	0.7500	0.7500	0.6787	0.5790	0.6436
Vo et al. [28] Navier	TBT	= 0	0.7332	0.7332	0.6706	0.5905	0.6467
	Present	≠0	0.7233	0.7233	0.6622	0.5840	0.6396
Vo et al. [28] FEM	TBT	= 0	0.7335	0.7335	0.6700	0.5907	0.6477
	Present	≠0	0.7291	0.7291	0.6661	0.5873	0.6439
SSPH	Present	≠0	0.7246	0.7234	0.6618	0.5840	0.6396
L/h = 20							
Li et al. [27]	TBT	= 0	0.7500	0.7500	0.6787	0.5790	0.6436
Vo et al. [28] Navier	TBT	= 0	0.7451	0.7451	0.6824	0.6023	0.6596
	Present	≠0	0.7432	0.7432	0.6809	0.6010	0.6583
Vo et al. [28] FEM	TBT	= 0	0.7470	0.7470	0.6777	0.6039	0.6682
	Present	≠0	0.7466	0.7466	0.6776	0.6036	0.6675
SSPH	Present	≠0	0.7425	0.7432	0.6789	0.6037	0.6606

Table 5
Verification studies of the developed meshless code for S-S FGB, dimensionless normal stress $\overline{\sigma}_z\left(\frac{L}{2},\frac{h}{2}\right)$ for various gradation exponents.

Method	Theory	ε_z	p = 0	p = 1	p = 2	p = 5	p = 10
L/h = 5							
Vo et al. [28] Navier	Present	≠0	0.1352	0.0670	0.0925	0.0180	−0.0181
Vo et al. [28] FEM	Present	≠0	0.1352	0.0672	0.0927	0.0183	−0.0179
SSPH	Present	≠0	0.1352	0.0671	0.0925	0.0182	−0.0180
L/h = 20							
Vo et al. [28] Navier	Present	≠0	0.0337	−0.5880	−0.6269	−1.1698	−1.5572
Vo et al. [28] FEM	Present	≠0	0.0338	−0.5874	−0.6261	−1.1690	−1.5560
SSPH	Present	≠0	0.0338	−0.5880	−0.6266	−1.1706	−1.5589

5.2.1. S-S Two-directional FG sandwich beams

Three types of two-directional FGBs (Type A, Type B and Type C) which have the boundary conditions as simply supported two directional FGB under uniformly distributed load are considered. Various gradation exponents in both directions and different aspect ratios are used to compute the dimensionless transverse deflections and stresses. As it is seen from Table 7, the computed maximum transverse deflection decreases as the aspect ratio increases. With the increasing of the gradation exponents in both directions, the transverse deflection values are increasing.

In Table 8, the dimensionless axial stress values are presented for various aspect ratios and gradation exponents. It is clear that the stress increases as the gradation exponent in the z direction increases. As it is expected, the axial stress value increases when the aspect ratio increases.

Table 6
Boundary conditions used for the numerical computations.

BC	x = 0	x = L
S-S	$u = 0, w_b = 0, w_s = 0, w_z = 0, M_x^b = 0, M_x^s = 0$	$u = 0$ *or* $N_x = 0, w_b = 0, w_s = 0, w_z = 0, M_x^b = 0, M_x^s = 0$
C-C	$u = 0, w_b = 0, w_s = 0, w_z = 0, w_b' = 0, w_s' = 0$	$u = 0, w_b = 0, w_s = 0, w_z = 0, w_b' = 0, w_s' = 0$
C-F	$u = 0, w_b = 0, w_s = 0, w_z = 0, w_b' = 0, w_s' = 0$	$N_x = 0, M_x^b = 0, M_x^s = 0, M_x^{b'} = 0, M_x^{s'} + Q_{xz} = 0, Q_{xz} = 0$

Table 7
The maximum transverse deflection of the S-S two-directional FG Sandwich Beams (Type A).

Aspect Ratio (L/h)	p_z	p_x				
		0	0.1	0.5	1	2
2	0	4.4752	4.5867	5.0566	5.6889	7.0829
	0.1	4.8908	5.0142	5.5164	6.1864	7.6508
	0.5	6.5541	6.6951	7.2875	8.0657	9.6541
	1	8.3858	8.5476	9.2249	9.9797	11.5627
	2	11.0281	11.1931	11.7844	12.5526	14.0412
5	0	3.1402	3.2165	3.5415	3.9711	4.9566
	0.1	3.4711	3.5542	3.9016	4.3687	5.3972
	0.5	4.7635	4.8636	5.2784	5.8191	6.9479
	1	6.1343	6.2412	6.6798	7.2342	8.3430
	2	7.8602	7.9617	8.3640	8.8636	9.8333
10	0	2.9455	3.0177	3.3215	3.7333	4.6555
	0.1	3.2622	3.3401	3.6655	4.1031	5.0682
	0.5	4.5015	4.5957	4.9843	5.4912	6.5521
	1	5.8035	5.9040	6.3124	6.8297	7.8657
	2	7.3967	7.4891	7.8588	8.3170	9.2137
20	0	2.8952	2.9659	3.2632	3.6662	4.5679
	0.1	3.2103	3.2867	3.6065	4.0367	4.9861
	0.5	4.4347	4.5274	4.9092	5.4076	6.4513
	1	5.7215	5.8206	6.2218	6.7299	7.7469
	2	7.2826	7.3734	7.7357	8.1853	9.0653

Table 8
The axial stress $\overline{\sigma}_x\left(\frac{L}{2}, \frac{h}{2}\right)$ of the S-S two-directional FG Sandwich Beams (Type A).

Aspect Ratio (L/h)	p_z	p_x				
		0	0.1	0.5	1	2
2	0	1.6260	1.6262	1.6258	1.6235	1.6144
	0.1	1.7367	1.7362	1.7331	1.7269	1.7094
	0.5	2.1407	2.1363	2.1171	2.0901	2.0297
	1	2.5312	2.5205	2.4765	2.4193	2.3026
	2	2.9921	2.9715	2.8865	2.7895	2.6000
5	0	3.8005	3.8009	3.8003	3.7945	3.7703
	0.1	4.0565	4.0554	4.0484	4.0338	3.9906
	0.5	4.9896	4.9794	4.9349	4.8718	4.7292
	1	5.8815	5.8566	5.7536	5.6196	5.3454
	2	6.8821	6.8347	6.6463	6.4155	5.9789
10	0	7.5287	7.5301	7.5306	7.5211	7.4775
	0.1	8.0237	8.0212	8.0057	7.9749	7.8852
	0.5	9.8766	9.5863	9.7674	9.6417	9.3574
	1	11.6349	11.5856	11.3818	11.1163	10.5730
	2	13.5902	13.4966	13.1246	12.6689	11.8073
20	0	15.0147	15.0165	15.0136	14.9895	14.8909
	0.1	16.0255	16.0204	15.9900	15.9313	15.7614
	0.5	19.7048	19.6642	19.4863	19.2343	18.6648
	1	23.2099	23.1113	22.7061	22.1731	21.0861
	2	27.1122	26.9255	26.1830	25.2728	23.5505

It is found in Table 9 that with the increasing of the gradation exponent in the x direction, the shear stress values are increasing. The dimensionless shear stress value decreases as the aspect ratio increases. It is clear in Table 10 that the dimensionless normal stress value almost vanishes as the aspect ratio increases (the gradation exponent in the z direction is set to zero).

In Table 11, the maximum dimensionless maximum transverse deflection values of type B FGB are given for the various types of sandwich structures, aspect ratios and gradation exponents. It is found that the computed deflection values increases as the gradation exponent in the z direction increases. For $p_z = 0$, the dimensionless maximum transverse deflection decreases as the thickness ratio of the middle layer increases with the increasing of the gradation exponent in the x direction.

The dimensionless maximum transverse deflections based on the sandwich beam with 2D-FG faces and ceramic core are presented for various types of sandwich structures, aspect ratios and gradation exponents in Table 12. It is clear that the transverse deflection value increases as the gradation exponent in the z direction increases. As it is expected, increasing of the thickness ratio of the ceramic layer in type C decreases the transverse deflection. It is observed that the maximum dimensionless deflection values obtained by using the FG structure as 2-2-1 are just between the values obtained by 1-1-1 and 1-2-1, as expected. It is clear that the maximum dimensionless deflection value decreases as the aspect ratio increases.

The variations of the dimensionless axial stress values with different thickness ratios are plotted in Fig. 3 for type B. For all configurations, the maximum tensile stress is obtained at the top (bottom) surface of the sandwich beam. The maximum axial stress increases as the gradation exponent in the x direction decreases on the top surface of the sandwich beam.

In Fig. 4, the dimensionless normal stress values are plotted through the thickness of the sandwich beam, type B. For all the

Table 9
The transverse shear stress $\overline{\sigma}_{xz}(0,0)$ of the S-S two-directional FG Sandwich Beams (Type A).

Aspect Ratio (L/h)	p_z	p_x				
		0	0.1	0.5	1	2
2	0	0.6834	0.6906	0.7189	0.7519	0.8085
	0.1	0.6900	0.6971	0.7249	0.7573	0.8122
	0.5	0.6990	0.7058	0.7318	0.7618	0.8107
	1	0.6829	0.6889	0.7119	0.7380	0.7791
	2	0.6246	0.6291	0.6460	0.6645	0.6923
5	0	0.7246	0.7318	0.7597	0.7923	0.8484
	0.1	0.7304	0.7374	0.7651	0.7973	0.8519
	0.5	0.7400	0.7465	0.7725	0.8022	0.8508
	1	0.7234	0.7295	0.7521	0.7780	0.8186
	2	0.6618	0.6668	0.6836	0.7017	0.7290
10	0	0.7496	0.7590	0.7961	0.8440	0.9437
	0.1	0.7434	0.7503	0.7774	0.8090	0.8622
	0.5	0.7532	0.7598	0.7852	0.8143	0.8617
	1	0.7361	0.7420	0.7644	0.7895	0.8291
	2	0.6739	0.6783	0.6946	0.7123	0.7386
20	0	0.7425	0.7498	0.7784	0.8125	0.8718
	0.1	0.7498	0.7571	0.7856	0.8194	0.8776
	0.5	0.7599	0.7667	0.7933	0.8240	0.8750
	1	0.7432	0.7493	0.7727	0.7993	0.8415
	2	0.6789	0.6835	0.7009	0.7199	0.7486

Table 10
The normal stress $\overline{\sigma}_z\left(\frac{L}{2},\frac{h}{2}\right)$ of the S-S two-directional FG Sandwich Beams (Type A).

Aspect Ratio (L/h)	p_z	p_x				
		0	0.1	0.5	1	2
2	0	0.3373	0.3373	0.3372	0.3367	0.3349
	0.1	0.3559	0.3558	0.3552	0.3541	0.3509
	0.5	0.4292	0.4283	0.4245	0.4192	0.4077
	1	0.5052	0.5029	0.4935	0.4815	0.4580
	2	0.5943	0.5897	0.5719	0.5507	0.5124
5	0	0.1352	0.1352	0.1351	0.1350	0.1346
	0.1	0.1074	0.1075	0.1082	0.1089	0.1106
	0.5	0.0562	0.0562	0.0568	0.0579	0.0611
	1	0.0671	0.0656	0.0604	0.0553	0.0498
	2	0.0925	0.0882	0.0730	0.0583	0.0422
10	0	0.0676	0.0676	0.0676	0.0675	0.0673
	0.1	−0.0114	−0.0111	−0.0098	−0.0077	−0.0030
	0.5	−0.1790	−0.1782	−0.1743	−0.1684	−0.1532
	1	−0.2083	−0.2099	−0.2150	−0.2183	−0.2144
	2	−0.2139	−0.2205	−0.2426	−0.2609	−0.2706
20	0	0.0338	0.0338	0.0338	0.0338	0.0337
	0.1	−0.1304	−0.1298	−0.1264	−0.1211	−0.1077
	0.5	−0.5025	−0.5005	−0.4913	−0.4776	−0.4431
	1	−0.5880	−0.5906	−0.5984	−0.6015	−0.5864
	2	−0.6266	−0.6388	−0.6791	−0.7108	−0.7197

Table 11
The maximum transverse deflections of the S-S two-directional FG Sandwich Beams (Type B).

p_x	p_z	L/h = 5				L/h = 20			
		1-1-1	1-2-1	1-8-1	2-2-1	1-1-1	1-2-1	1-8-1	2-2-1
0	0	3.1402	3.1402	3.1402	3.1402	2.8952	2.8952	2.8952	2.8952
	0.1	3.2319	3.2647	3.3633	3.2281	2.9705	3.0036	3.1033	2.9587
	0.5	3.5665	3.7089	4.1666	3.5564	3.2475	3.3872	3.8441	3.2129
	1	3.9204	4.1632	4.9663	3.9185	3.5512	3.7820	4.5694	3.4559
	2	4.4795	4.8517	6.0529	4.5100	4.0426	4.3525	5.5161	3.9168
0.1	0	3.1738	3.1699	3.1566	3.1761	2.9290	2.9258	2.9121	2.9302
	0.1	3.2680	3.2976	3.3825	3.2652	3.0055	3.0358	3.1222	2.9946
	0.5	3.6072	3.7473	4.1929	3.5979	3.2866	3.4249	3.8702	3.2459
	1	3.9636	4.2062	4.9984	3.9629	3.5934	3.8235	4.6015	3.4977
	2	4.5262	4.8981	6.0882	4.5572	4.0876	4.3984	5.5521	3.9889
0.5	0	3.3177	3.2961	3.2219	3.3282	3.0680	3.0492	2.9770	3.0751
	0.1	3.4148	3.4288	3.4554	3.4190	3.1475	3.1648	3.1967	3.1412
	0.5	3.7690	3.9000	4.2943	3.7657	3.4452	3.5758	3.9707	3.4012
	1	4.1395	4.3762	5.1223	4.1427	3.7644	3.9902	4.7252	3.6683
	2	4.7134	5.0815	6.2272	4.7483	4.2697	4.5834	5.6906	4.1249
1	0	3.5023	3.4530	3.2971	3.5272	3.2476	3.2038	3.0517	3.2666
	0.1	3.6000	3.5911	3.5396	3.6165	3.3283	3.3248	3.2782	3.3306
	0.5	3.9745	4.0902	4.4116	3.9806	3.6467	3.7635	4.0872	3.6065
	1	4.3592	4.5853	5.2673	4.3703	3.9806	4.1973	4.8687	3.8897
	2	4.9463	5.3046	6.3883	4.9875	4.4975	4.8125	5.8502	4.3698
2	0	3.8760	3.7547	3.4258	3.9431	3.6143	3.5019	3.1791	3.6706
	0.1	3.9704	3.9025	3.6842	4.0201	3.6922	3.6322	3.4214	3.7229
	0.5	4.3826	4.4539	4.6148	4.4178	4.0507	4.1256	4.2887	4.0308
	1	4.7919	4.9847	5.5178	4.8292	4.4091	4.5943	5.1177	4.3463
	2	5.3917	5.7219	6.6645	5.4564	4.9371	5.2373	6.1249	4.8377

Table 12
The maximum transverse deflections of the S-S two-directional FG Sandwich Beams (Type C).

p_x	p_z	L/h = 5				L/h = 20			
		1-1-1	1-2-1	1-8-1	2-2-1	1-1-1	1-2-1	1-8-1	2-2-1
0	0	13.7597	10.3450	5.0616	11.7408	13.4506	10.0800	4.8017	11.4238
	0.1	11.5719	8.9629	4.8170	10.0642	11.2682	8.6934	4.5568	9.7633
	0.5	7.8402	6.4901	4.2556	7.1171	7.5572	6.2234	3.4000	6.8266
	1	6.2095	5.3611	3.9321	5.7775	5.9373	5.0983	3.6789	5.5046
	2	4.9737	4.4839	3.6449	4.7393	4.7119	4.2269	3.3941	4.4783
0.1	0	12.4834	9.6719	4.9708	10.7770	12.1706	9.4059	4.7111	10.4790
	0.1	10.7054	8.4885	4.7401	9.4128	10.3994	8.2165	4.4818	9.1047
	0.5	7.5039	6.2886	4.2112	6.8473	7.2199	6.0221	3.9561	6.5597
	1	6.0343	5.2502	3.9030	5.6327	5.7613	4.9879	3.6501	5.3608
	2	4.8871	4.4286	3.6275	4.6673	4.6274	4.1711	3.3772	4.4070
0.5	0	9.4397	7.8718	4.6673	8.4185	9.1206	7.6106	4.4108	8.1127
	0.1	8.4793	7.1439	4.4862	7.6764	8.1706	6.8700	4.2298	7.3680
	0.5	6.5069	5.6587	4.0580	6.0408	6.2253	5.3945	3.8040	5.7569
	1	5.4735	4.8856	3.8004	5.1692	5.2055	4.6256	3.5490	4.9004
	2	4.6040	4.2344	3.5666	4.4251	4.3451	3.9800	3.3169	4.1669
1	0	7.5490	6.6017	4.3873	6.9846	7.2296	6.3437	4.1323	6.7955
	0.1	6.9827	6.1379	4.2462	6.4602	6.6753	5.8568	3.9922	6.1562
	0.5	5.7178	5.1238	3.9088	5.3861	5.4388	4.8611	3.6551	5.1050
	1	4.9904	4.5528	3.6976	4.7624	4.7252	4.2959	3.4477	4.4948
	2	4.3387	4.0486	3.5031	4.1978	4.0816	3.7958	3.2549	3.9396
2	0	5.7615	5.2893	4.0154	5.4086	5.4296	5.0292	3.7635	5.2302
	0.1	5.4854	5.0452	3.9241	5.2058	5.1789	4.9130	3.6723	4.9122
	0.5	4.8192	4.4731	3.6960	4.6212	4.5439	4.2129	3.4455	4.3456
	1	4.3952	4.1214	3.5475	4.2499	4.1325	3.8677	3.3012	3.9833
	2	3.9824	3.7913	3.4100	3.8886	3.7303	3.5412	3.1634	3.6276

types of skin-core-skin thickness ratios except 1-8-1, the maximum normal stress on the top surface of the sandwich beam increases as the gradation exponent in the x direction increases. However, it is interesting that the normal stress value decreases at the top surface of the 1-8-1 sandwich beam as the gradation exponent in the x direction increases.

It is clear in Fig. 5 that the maximum shear stress is obtained by setting the gradation exponent in the x direction as 5 for all skin-core-skin thickness ratios of type B. As it is expected, the shear stress value is zero at the top and bottom surfaces of the sandwich beam. It is also interesting that there is a sudden drop for the shear stress value at a point which is located between the core (1D FG) and the top skin (2D FG).

As it is seen in Fig. 6 plotted for the variation of the axial stress for Type C, the axial stress value increases on the top and bottom surfaces of the beam as the gradation exponent in the x

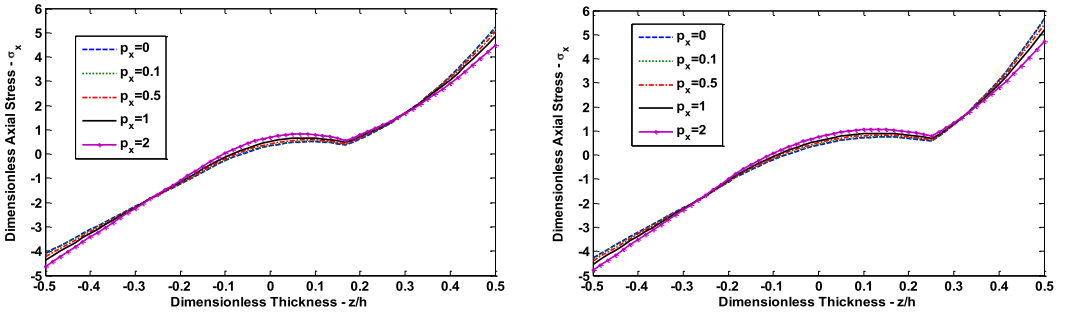

a) Symmetric scheme (1-1-1) b) Symmetric scheme (1-2-1)

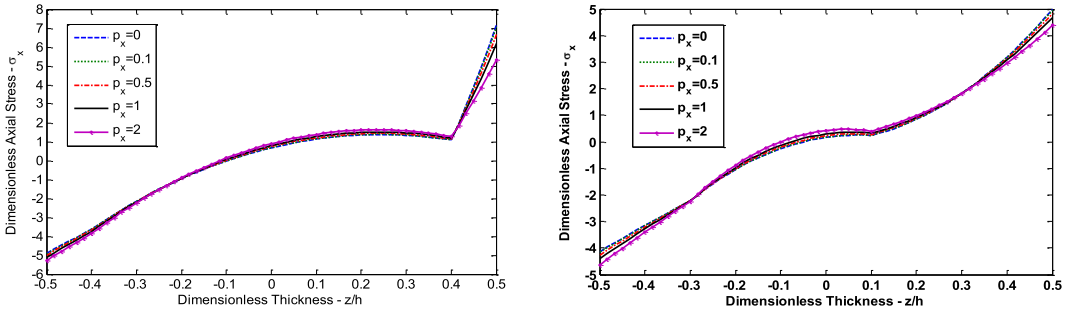

d) Symmetric scheme (1-8-1) c) Non-symmetric scheme (2-2-1)

Fig. 3. Variation of the axial stress $\overline{\sigma}_x\left(\frac{L}{2}, z\right)$ of FG S-S beams under uniform load (p_x = 2, L/h = 5, Type B).

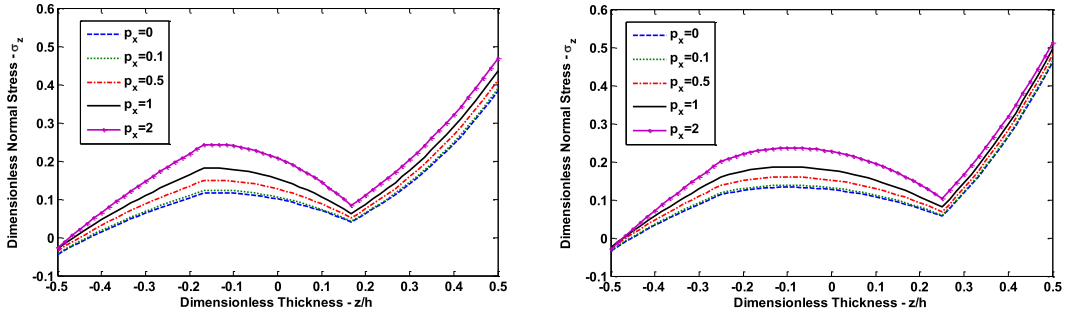

b) Symmetric scheme (1-1-1) a) Symmetric scheme (1-2-1)

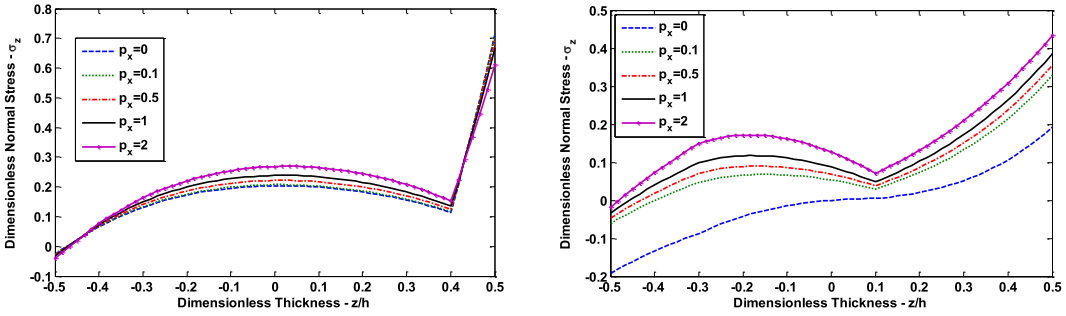

d) Symmetric scheme (1-8-1) c) Non-symmetric scheme (2-2-1)

Fig. 4. Variation of the normal stress $\overline{\sigma}_z\left(\frac{L}{2}, z\right)$ of FG S-S beams under uniform load (p_x = 2, L/h = 5, Type B).

direction increases. However, the maximum axial stress values are observed around the skin to core transition zone except for the non-symmetric sandwich beam. The maximum axial stress is obtained around the transition zone which is between to lower skin and the core for 2-2-1 non-symmetric sandwich beam of type C.

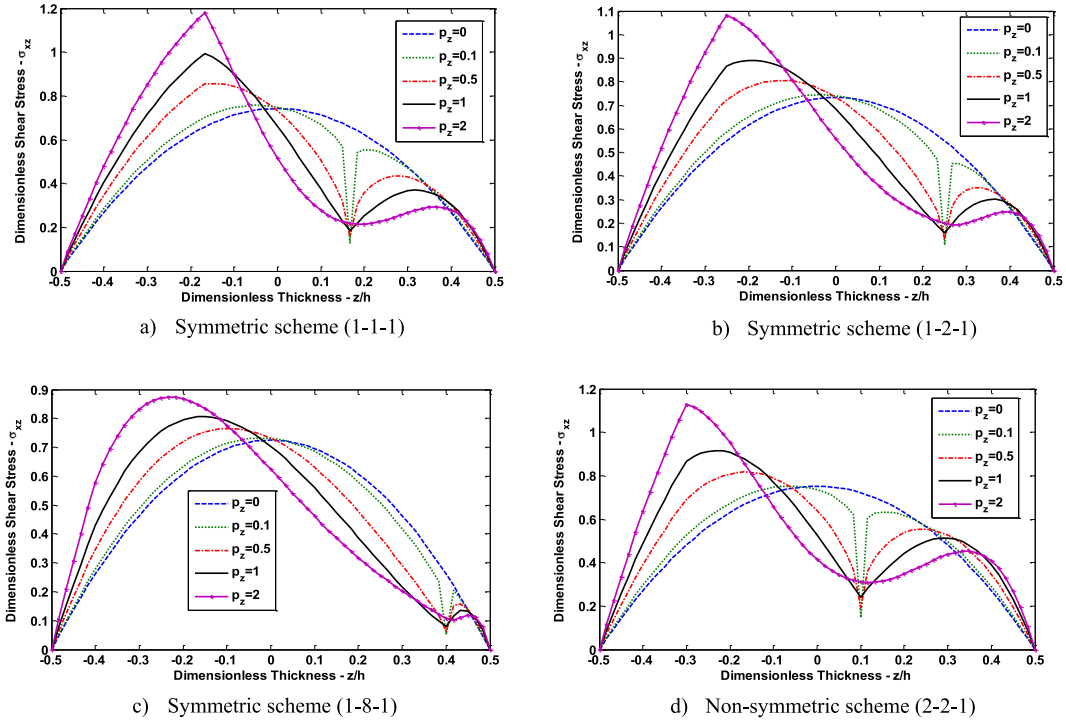

a) Symmetric scheme (1-1-1) b) Symmetric scheme (1-2-1)

c) Symmetric scheme (1-8-1) d) Non-symmetric scheme (2-2-1)

Fig. 5. Variation of the shear stress $\overline{\sigma}_{xz}(0,z)$ of FG S-S beams under uniform load (p_z = 1, L/h = 5, Type B).

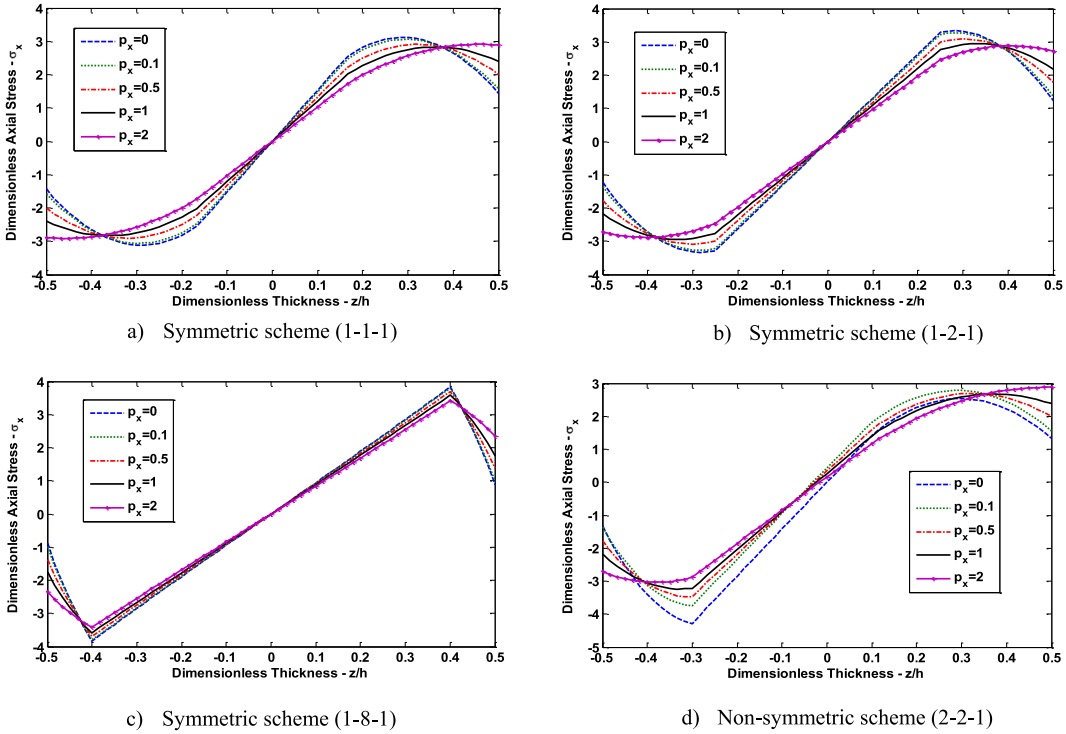

a) Symmetric scheme (1-1-1) b) Symmetric scheme (1-2-1)

c) Symmetric scheme (1-8-1) d) Non-symmetric scheme (2-2-1)

Fig. 6. Variation of the axial stress $\overline{\sigma}_x\left(\frac{L}{2},z\right)$ of FG S-S beams under uniform load (p_x = 2, L/h = 5, Type C).

The variations of the normal stress values are plotted in Fig. 7 for different gradation exponents and skin-core-skin ratios. For all configurations, expect 2-2-1 with p_x = 10, the maximum normal stresses are obtained around the skin to core transition zone. However, for the 2-2-1 with p_x = 10, the maximum normal stress values are obtained at the top and bottom surfaces of the sandwich beam.

In Fig. 8, the maximum dimensionless shear stress values are plotted for various gradation exponents in the z direction. It is interesting to see that the maximum shear stress for both symmetric and non-symmetric sandwich beams occurs at the middle plane of the beam. As the gradation exponent in the z direction increases the shear stress value decreases.

5.2.2. C-C Two-directional FG sandwich beam

The dimensionless maximum transverse deflections and the axial, normal and shear stresses of the clamped-clamped FG sand-

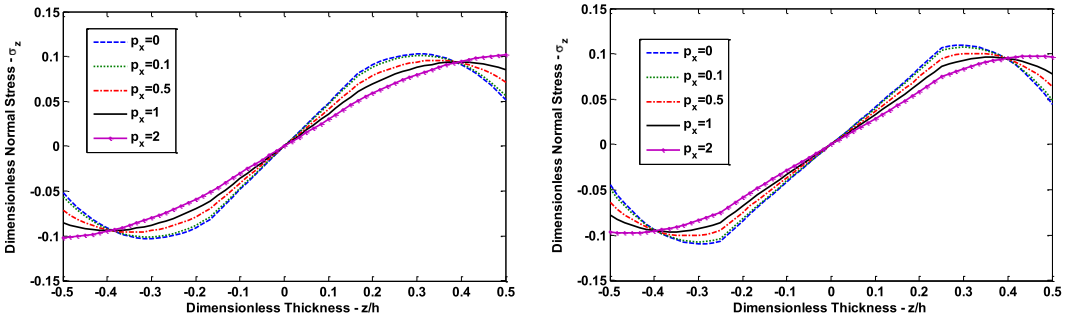

a) Symmetric scheme (1-1-1) b) Symmetric scheme (1-2-1)

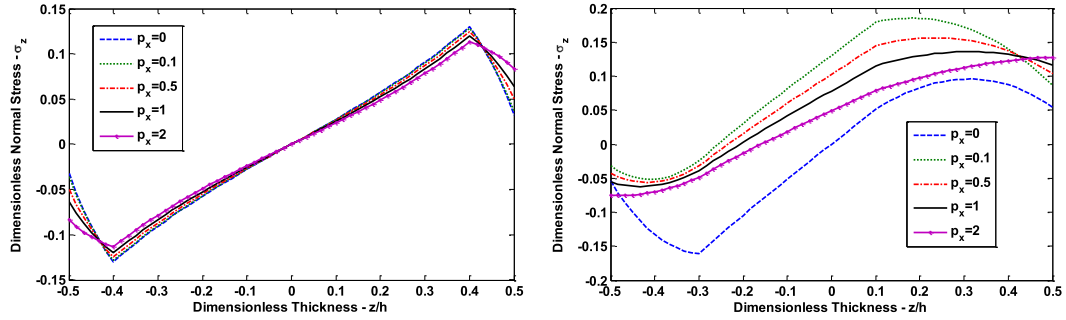

c) Symmetric scheme (1-8-1) d) Non-symmetric scheme (2-2-1)

Fig. 7. Variation of the normal stress $\overline{\sigma}_z\left(\frac{L}{2}, z\right)$ of FG S-S beams under uniform load (p_x = 2, L/h = 5, Type C).

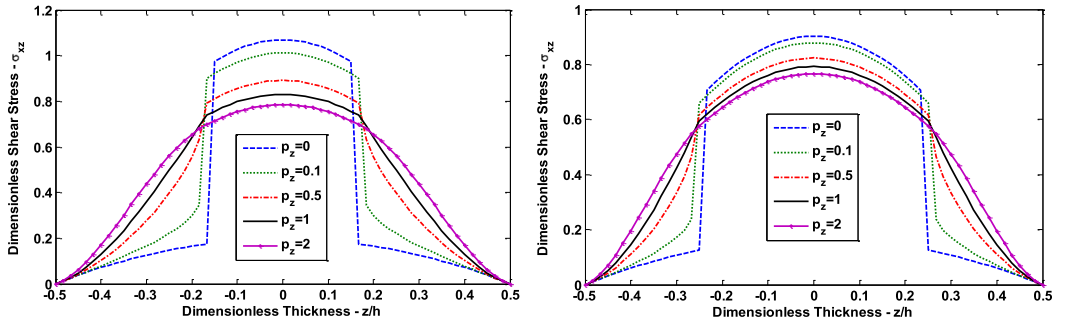

a) Symmetric scheme (1-1-1) b) Symmetric scheme (1-2-1)

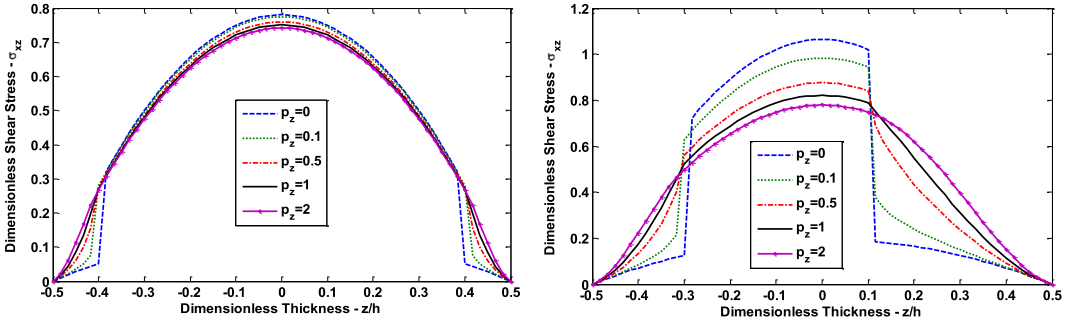

c) Symmetric scheme (1-8-1) d) Non-symmetric scheme (2-2-1)

Fig. 8. Variation of the shear stress $\overline{\sigma}_{xz}(0, z)$ of FG S-S beams under uniform load (p_z = 1, L/h = 5, Type C).

wich beam are investigated for type B and type C structures. The results are given in Tables 13 and 14 and Fig. 9.

It is found in Table 13 that the computed transverse deflection value increases as the gradation exponent in the z direction increases. For p_z = 0, the dimensionless maximum transverse deflection decreases as the thickness ratio of the middle layer increases with the increasing of the gradation exponent in the x direction.

In Table 14, the dimensionless maximum transverse deflections of the sandwich beam, type C, are presented for various aspect rations, gradation exponents in both directions and different

Table 13
The maximum transverse deflections of the C-C two-directional FG Sandwich Beams (Type B).

p_x	p_z	L/h = 5				L/h = 20			
		1-1-1	1-2-1	1-8-1	2-2-1	1-1-1	1-2-1	1-8-1	2-2-1
0	0	0.8349	0.8349	0.8349	0.8349	0.5898	0.5898	0.5898	0.5898
	0.1	0.8670	0.8729	0.8922	0.8715	0.6058	0.6124	0.6323	0.6040
	0.5	0.9799	1.0059	1.1125	1.0085	0.6667	0.6925	0.7833	0.6561
	1	1.0620	1.1337	1.3272	1.1625	0.7291	0.7729	0.9321	0.7138
	2	1.2564	1.3703	1.6542	1.3897	0.8273	0.8970	1.1291	0.8106
0.1	0	0.8433	0.8422	0.8379	0.8442	0.5971	0.5964	0.5934	0.5974
	0.1	0.8751	0.8812	0.8963	0.8812	0.6133	0.6192	0.6363	0.6117
	0.5	0.9905	1.0401	1.0892	1.0196	0.6842	0.7001	0.7887	0.6647
	1	1.1154	1.1646	1.3292	1.1763	0.7352	0.7819	0.9389	0.7230
	2	1.2656	1.3617	1.6543	1.3914	0.8373	0.9068	1.1368	0.8204
0.5	0	0.8765	0.8700	0.8529	0.8812	0.6259	0.6216	0.6066	0.6272
	0.1	0.9098	0.9108	0.9126	0.9202	0.6432	0.6462	0.6511	0.6428
	0.5	1.0410	1.0434	1.1412	1.0596	0.7057	0.7314	0.8093	0.6991
	1	1.1443	1.1758	1.3392	1.2035	0.7651	0.8189	0.9643	0.7597
	2	1.3366	1.4308	1.6848	1.4035	0.8766	0.9450	1.1656	0.8597
1	0	0.9161	0.9053	0.8686	0.9271	0.6610	0.6519	0.6209	0.6650
	0.1	0.9533	0.9462	0.9308	0.9649	0.6806	0.6787	0.6674	0.6824
	0.5	1.0778	1.0595	1.1739	1.1148	0.7470	0.7694	0.8320	0.7423
	1	1.1945	1.2603	1.4025	1.2256	0.8164	0.8596	0.9923	0.8054
	2	1.3587	1.4592	1.7128	1.5048	0.9254	0.9900	1.1970	0.9080
2	0	0.9784	0.9596	0.8938	1.0058	0.7279	0.7064	0.6439	0.7389
	0.1	1.0286	1.0080	0.9588	1.0662	0.7505	0.7360	0.6934	0.7594
	0.5	1.1574	1.1599	1.1856	1.1935	0.8239	0.8368	0.8685	0.8294
	1	1.2749	1.3221	1.4290	1.3663	0.8977	0.9336	1.0373	0.8926
	2	1.4465	1.5462	1.7667	1.5917	1.0038	1.0672	1.2464	0.9962

Table 14
The maximum transverse deflections of the C-C two-directional FG Sandwich Beams (Type C).

p_x	p_z	L/h = 5				L/h = 20			
		1-1-1	1-2-1	1-8-1	2-2-1	1-1-1	1-2-1	1-8-1	2-2-1
0	0	3.0687	2.3400	1.2521	2.6572	2.6921	2.0196	0.9723	2.2951
	0.1	2.6198	2.0587	1.2014	2.3013	2.2539	1.7270	0.9234	1.9596
	0.5	1.8359	1.5487	1.0796	1.6899	1.5298	1.2587	0.8121	1.3874
	1	1.4933	1.3115	1.0094	1.4061	1.2016	1.0327	0.7481	1.1174
	2	1.2311	1.1265	0.9472	1.1825	0.9554	0.8580	0.6922	0.9120
0.1	0	2.7982	2.1951	1.2321	2.4789	2.4284	1.8804	0.9533	2.1007
	0.1	2.4305	1.9559	1.1824	2.2046	2.0753	1.6396	0.9077	1.8245
	0.5	1.7642	1.5040	1.0686	1.6311	1.4620	1.2172	0.8030	1.3356
	1	1.4552	1.2865	1.0026	1.3714	1.1650	1.0097	0.7422	1.0883
	2	1.2108	1.1142	0.9424	1.1653	0.9378	0.8465	0.6891	0.8983
0.5	0	2.1958	1.8353	1.1648	1.9802	1.8446	1.5321	0.8932	1.6559
	0.1	1.9858	1.6810	1.1265	1.8104	1.6482	1.3839	0.8572	1.4934
	0.5	1.5574	1.3703	1.0352	1.4622	1.2333	1.0989	0.7726	1.1470
	1	1.3351	1.2079	0.9794	1.2733	1.0580	0.9385	0.7224	1.0167
	2	1.1506	1.0708	0.9288	1.1123	0.8825	0.8094	0.6835	0.8826
1	0	1.8405	1.5948	1.1085	1.7057	1.5060	1.3033	0.8410	1.3890
	0.1	1.7019	1.4902	1.0774	1.5903	1.3804	1.2032	0.8127	1.2779
	0.5	1.4053	1.2669	1.0046	1.3330	1.1099	0.9856	0.7451	1.0410
	1	1.2405	1.1423	0.9571	1.1924	0.9476	0.8822	0.7051	0.9078
	2	1.0965	1.0329	0.9153	1.0674	0.8389	0.7777	0.6555	0.7934
2	0	1.5091	1.3610	1.0402	1.4299	1.1979	1.0790	0.7760	1.1246
	0.1	1.4271	1.2953	1.0182	1.3603	1.1250	1.0178	0.7564	1.0614
	0.5	1.2413	1.1497	0.9646	1.1956	0.9597	0.8808	0.7111	0.9141
	1	1.1316	1.0640	0.9300	1.0932	0.8611	0.8000	0.6699	0.8267
	2	1.0313	0.9851	0.8975	1.0086	0.7681	0.7253	0.6446	0.7462

skin-core-skin thickness ratios. It is clear that the transverse deflection value increases as the gradation exponent in the z direction increases. As it is expected, the increasing of the ceramic content of the structure decreases the transverse deflection value. It is observed that the maximum dimensionless transverse deflection values obtained by using the 2-2-1 structure are just between the values obtained by 1-1-1 and 1-2-1, as expected. It is clear that the maximum dimensionless transverse deflection value decreases as the aspect ratio increases.

As it is seen in Fig. 9, the axial stress increases as the gradation exponent in the x direction increases at the top and the bottom surfaces of the sandwich beam. However, the maximum axial stress values are observed around the transition zone which is between the upper (lower) skin and the core with the gradation exponent in the x direction as $p_x = 0$. The similar case is valid for the normal stress as well. Based on the values of the dimensionless shear stress plotted in Fig. 9, the maximum shear stress is obtained in the middle plane of the beam. As it is expected, the shear stress

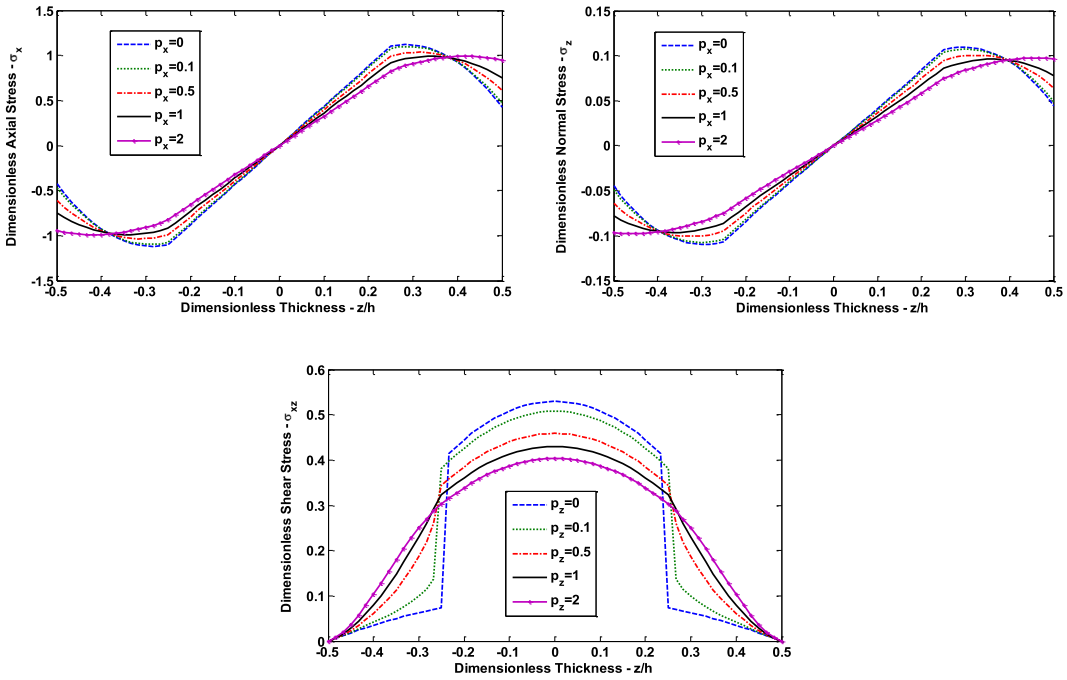

Fig. 9. Variation of the stresses $\overline{\sigma}_x\left(\frac{L}{2},z\right)$, $\overline{\sigma}_z\left(\frac{L}{2},z\right)$, $\overline{\sigma}_{xz}(0,z)$ of FG C-C beams under uniform load ($p_x = 2$, $p_z = 1$, L/h = 5, 1-2-1, Type C).

Table 15
The maximum transverse deflections of the C-F two-directional FG Sandwich Beams (Type B).

p_x	p_z	L/h = 3				L/h = 5			
		1-1-1	1-2-1	1-8-1	2-2-1	1-1-1	1-2-1	1-8-1	2-2-1
0	0	30.8511	30.8511	30.8511	30.8511	27.6636	27.6636	27.6636	27.6636
	0.1	32.3478	32.7501	33.9527	32.2990	28.6873	29.2354	31.0260	28.5773
	0.5	35.7137	37.2101	42.0063	35.6116	31.3358	32.9204	38.4992	30.9358
	1	39.2977	41.8099	50.0417	39.2827	34.3117	36.8200	45.9049	33.6296
	2	44.9406	48.7686	60.9201	45.2819	39.3970	43.0553	55.7854	38.3142
0.1	0	31.9015	31.9312	32.1886	31.9225	29.7702	30.0227	30.7079	29.6378
	0.1	32.6318	32.9688	34.0822	32.6406	30.0224	30.6333	31.3462	30.0124
	0.5	35.9236	37.3989	42.1233	35.8415	31.8002	33.3152	38.6997	31.4718
	1	39.4960	42.0062	50.0447	39.5118	34.7104	37.1800	46.1141	34.0828
	2	45.1448	48.9810	61.0762	45.5134	39.7536	43.3838	55.9978	38.7176
0.5	0	32.3621	32.4822	32.3431	32.4202	30.2258	30.3661	30.8084	30.1554
	0.1	33.2068	33.4876	34.3491	33.1846	30.6396	31.0142	32.0980	30.5481
	0.5	36.6291	38.0511	42.5134	36.5549	33.1028	34.5173	39.3815	32.7825
	1	40.2727	42.7318	50.6819	40.2367	36.0320	38.4108	46.8644	35.4589
	2	45.9509	49.7111	61.6227	46.3479	41.0354	44.5865	56.7859	40.1049
1	0	33.1494	32.9736	32.6014	33.2488	30.9957	30.9402	30.9759	31.0388
	0.1	33.7845	34.0449	34.7391	33.8189	31.4203	31.7327	32.6091	31.3393
	0.5	37.3937	38.8305	43.0492	37.3187	34.2625	35.6295	40.0856	33.9110
	1	41.1322	43.6099	51.2829	41.1621	37.3461	39.6738	47.6815	36.7622
	2	46.9412	50.6149	62.2880	47.2804	42.4078	45.8940	57.6630	41.5255
2	0	34.9285	34.3365	33.1248	35.3033	32.8736	32.3082	31.3750	32.8887
	0.1	35.0174	35.1077	35.3151	35.5457	33.3542	32.9383	33.2750	33.2281
	0.5	38.8406	40.1626	44.0390	38.8570	36.1435	37.3791	41.1898	35.8202
	1	42.8227	45.2932	52.5661	42.8472	39.4876	41.7319	49.0417	38.9134
	2	48.8797	52.6239	63.6040	49.1244	44.7043	48.0935	59.1517	43.8744

value is zero at top and the bottom surfaces of the beam. The maximum shear stress increases as the gradation exponent in the z direction decreases.

5.2.3. C-F Two-directional FG sandwich beam

Finally, the results of elastostatic analysis of the C-F FG sandwich beam under uniformly distributed load are obtained for various gradation exponents and aspect ratios. For this example, accurate and agreed results cannot be obtained when the aspect ratio is greater than 5 and the gradation exponent in the x direction is greater than 2. This point is crucial to determine future studies based on the present quasi-3D shear deformation theory and the SSPH method. It is not clear that increasing the gradation exponent in the x direction deteriorates the accuracy of the present quasi-3D theory when employing higher aspect ratios. For this example, two different aspect ratios are employed to investigate the inefficiency of the present theory and the numerical method. It is not found a concrete reason that may explain the loss of accuracy when the aspect ratio is set to above 5. However, the developed SSPH code works very well for the aspect ratio lower than 6.

As it is seen from Table 15, the maximum transverse deflection increases as the gradation exponent in the z direction increases for

Table 16
The maximum transverse deflections of the C-F two-directional FG Sandwich Beams (Type C).

p_x	p_z	L/h = 3				L/h = 5			
		1-1-1	1-2-1	1-8-1	2-2-1	1-1-1	1-2-1	1-8-1	2-2-1
0	0	136.9991	103.3784	50.3014	118.0826	127.6384	96.6263	43.1688	113.0070
	0.1	115.3140	89.5492	47.8237	101.4237	106.7625	82.7347	41.0276	96.7551
	0.5	78.2025	64.7501	42.1990	72.0151	70.8790	58.1097	36.0461	68.2075
	1	61.8945	53.3634	38.9498	58.6490	55.1374	47.0225	33.1415	55.4228
	2	49.4529	44.5126	36.0325	48.3508	43.2444	38.5398	30.5694	45.6642
0.1	0	133.4669	101.7698	50.2666	114.9350	122.4045	93.8669	42.6404	108.2332
	0.1	113.0266	88.4514	47.7988	99.6256	103.1453	80.6911	40.6110	93.7119
	0.5	74.4259	64.3347	42.1831	71.2924	69.3732	57.1657	35.8266	66.8920
	1	61.4878	53.1647	38.9020	58.3130	54.3137	46.4849	33.0055	54.6829
	2	49.2967	44.4487	36.0371	48.1423	42.8319	38.2668	30.4942	45.2804
0.5	0	121.9465	95.8655	49.7060	105.1019	104.9075	83.7009	40.2252	92.7760
	0.1	105.2029	84.2960	47.3493	93.2968	90.5026	72.9827	38.7195	82.7805
	0.5	74.4014	62.6153	41.9403	68.4383	63.6496	53.4150	34.8321	61.3354
	1	59.9906	52.2866	38.7884	56.6631	51.0425	44.2826	32.3947	51.2206
	2	48.6458	44.0517	35.9585	47.2989	41.1472	37.1179	30.1566	43.3719
1	0	110.0557	89.0003	48.6191	90.9987	87.9811	72.6506	37.2154	64.7954
	0.1	96.6748	79.2645	46.5284	83.0437	77.6217	64.4714	36.3421	63.9215
	0.5	70.7806	60.4115	41.5131	61.5324	57.3192	49.0825	33.5601	57.2458
	1	58.0489	51.0888	38.5053	50.6997	47.2790	41.6715	31.6014	51.4485
	2	47.7180	43.4621	35.8174	43.7508	39.1340	35.7019	29.7120	44.3256
2	0	88.5473	74.8915	45.8780	81.1447	63.8857	55.1042	31.9012	63.2332
	0.1	80.7093	68.9819	44.4299	76.6237	58.3723	50.6618	32.0742	62.4496
	0.5	63.6103	55.8076	40.4401	62.0931	47.0441	41.7644	31.2084	56.6573
	1	54.0877	48.5051	37.8609	53.1952	40.9234	37.1261	30.1039	50.5046
	2	45.7781	42.1696	35.4481	45.6600	35.5964	33.1584	28.8526	43.2953

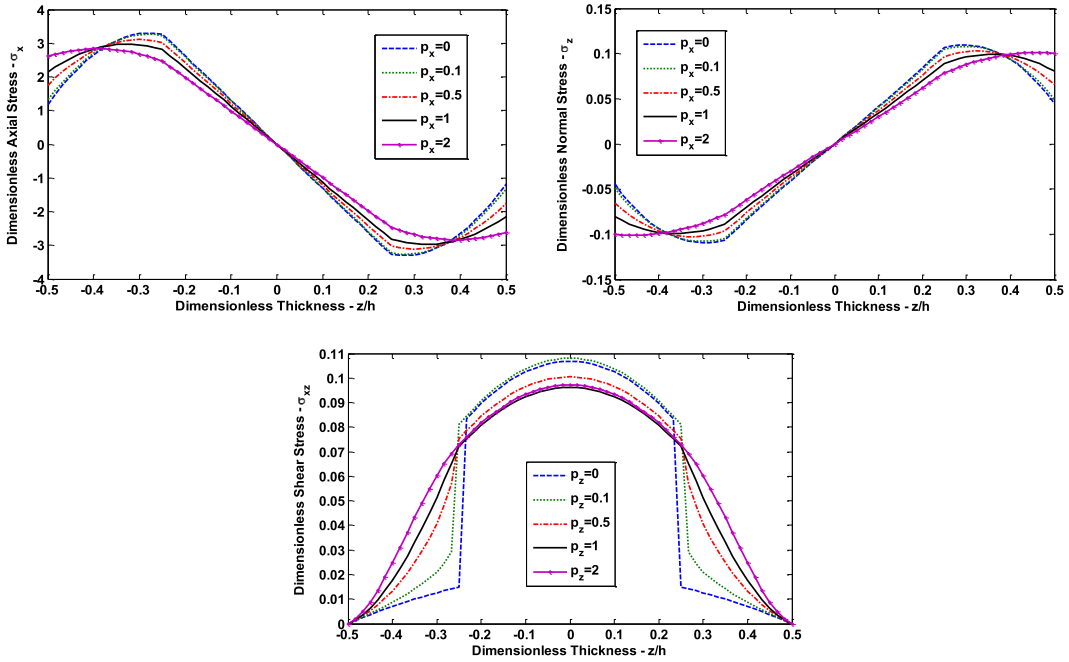

Fig. 10. Variation of the stresses $\overline{\sigma}_x(\frac{L}{2},z)$, $\overline{\sigma}_z(\frac{L}{2},z)$, $\overline{\sigma}_{xz}(0,z)$ of FG C-F beams under uniform load ($p_x = 2$, $p_z = 1$, L/h = 5, 1-2-1, Type C).

type B. For $p_z = 0$, the dimensionless maximum dimensionless deflection decreases as the thickness ratio of the middle layer increases with the increasing of the gradation exponent in the x direction.

In Table 16, the dimensionless transverse deflections are presented based on the various aspect ratios, gradation exponents in both directions and different types of skin-core-skin thickness ratios. It is observed that either the gradation exponent in the x direction or the gradation exponent in the z direction increases the transverse deflection decreases. As it is expected, by increasing of the ceramic volume, the deflections are decreasing. It is found that the maximum dimensionless deflection values obtained by using the FG structure as 2-2-1 are just between the values obtained by 1-1-1 and 1-2-1, as expected.

It is observed in Fig. 10 that the dimensionless axial stress value computed by using quasi-3D formulation increases as the gradation exponent in the x direction decreases. However, the maximum axial stress values are observed around the transition zone which is between the upper (lower) skin and the core (with the gradation exponent in the x direction as $p_x = 0$). The similar case is valid for

the normal stress as well. Based on the values of the dimensionless shear stress plotted in Fig. 10, the maximum shear stress is obtained in the middle plane of the beam. As it is expected, the shear stress value is zero at top and bottom surfaces of the beam. It is interesting that the maximum shear stress with $p_x = 2$ is obtained when the gradation exponent in the z direction is set to 0.1.

6. Conclusion

The static behaviour of the two directional functionally graded sandwich beams subjected to different sets of boundary conditions and uniformly distributed load are investigated by employing the SSPH basis functions and using strong formulation of the problem. A quasi-3D theory which includes both shear deformation and thickness stretching effect is used to evaluate the transverse deflections, axial, normal and shear stresses of two directional FG sandwich beams. The developed code is verified by studying a simply supported conventional FGB problem and comparing the results with previous studies and the analytical solutions.

Three different boundary conditions are considered with different gradation exponents in both directions and various aspect ratios. The effect of the normal strain is investigated and it is found that it is important and should be considered in the static behaviour of the two directional functionally graded sandwich beams.

Another important point is that for CF beam, the computed results by employing the aspect ratio higher than 5 are not agree very well with the previous studies as the gradation exponent in the x direction is set to higher than 2. At least within the scope of this work, it may be told that by using the SSPH method and present quasi-3D theory, it is not recommended to use the gradation exponent in the x direction greater than 2 as the aspect ratio increases with CF boundary condition. This situation should be investigated in future studies.

It is found that the SSPH method provides satisfactory results at least for the problems studied here. Based on the results of three numerical examples it is recommended that the SSPH method can be applied for solving linear two directional functionally graded sandwich beam problems by employing a quasi-3D theory.

References

[1] Kadoli R, Akhtar K, Ganesan N. Static analysis of functionally graded beams using higher order shear deformation theory. Appl Math Model 2008;32:2509–25.
[2] Li XF. A unified approach for analyzing static and dynamic behaviors of functionally graded Timoshenko and Euler-Bernoulli beams. J Sound Vib 2008;318:1210–29.
[3] Benatta MA, Mechab I, Tounsi A, Abbas ABE. Static analysis of functionally graded short beams including warping and shear deformation effects. Comput Mater Sci 2008;44:765–73.
[4] Ben-Oumrane S, Tounsi A, Mechab I, Mohamed BB, Mustapha M, Abbas ABE. Theoretical analysis of flexional bending of Al/Al_2O_3 S-FGM thick beams. Comput Mater Sci 2009;44:1344–50.
[5] Menaa R, Tounsi A, Mouaici F, Mechab I, Zidi M, Bedia EAA. Analytical solutions for static shear correction factor of functionally graded rectangular beams. Mech Adv Mater Struct 2012;19:641–52.
[6] Li SR, Cao DF, Wan ZQ. Bending solutions of FGM Timoshenko beams from those of the homogenous Euler-Bernoulli beams. Appl Math Model 2013;37:7077–85.
[7] Jing LL, Ming PJ, Zhang WP, Fu LR, Cao YP. Static and free vibration analysis of functionally graded beams by combination Timoshenko theory and finite volume method. Compos Struct 2016;138:192–213.
[8] Aydogdu M, Taskin V. Free vibration analysis of functionally graded beams with simply supported edges. Mater Des 2007;28:1651–6.
[9] Sina SA, Navazi HM, Haddadpour H. An analytical method for free vibration analysis of functionally graded beams. Materials&Design 2009;30:741–7.
[10] Simsek M. Fundamental frequency analysis of functionally graded beams by using different higher-order beam theories. Nucl Eng Des 2010;240:697–705.
[11] Simsek M, Kocaturk T. Free and forced vibration of a functionally graded beam subjected to a concentrated moving harmonic load. Compos Struct 2009;90:465–73.
[12] Simsek M. Vibration analysis of a functionally graded beam under a moving mass by using different beam theories. Compos Struct 2010;92:904–17.
[13] Sanjay AK, Gupta RK, Ramachandran P, Venkateswara RG. Free vibration analysis of functionally graded beams. Def Sci J 2012;62(3):139–46.
[14] Mahi A, Adda Bedia EA, Tounsi A, Mechab I. An analytical method for temperature-dependent free vibration analysis of functionally graded beams with general boundary conditions. Compos Struct 2010;92:1877–87.
[15] Pradhan KK, Chakraverty S. Free vibration of Euler and Timoshenko functionally graded beams by Rayleigh-Ritz method. Compos B 2013;51:175–84.
[16] Pradhan KK, Chakraverty S. Effects of different shear deformation theories on free vibration of functionally graded beams. Int J Mech Sci 2014;82:149–60.
[17] Nuttawit W, Variddhi U. Free vibration analysis of functionally graded beams with general elastically end constraints by DTM. World J Mech 2012;2:297–310.
[18] Su H, Banerjee JR, Cheung CW. Dynamic stiffness formulation and free vibration analysis of functionally graded beams. Compos Struct 2013;106:854–62.
[19] Li SR, Wan ZG, Zhang JH. Free vibration of functionally graded beams based on both classical and first-order shear deformation beam theories. Appl Math Mech 2014;35:591–606.
[20] Aydogdu M. Thermal buckling analysis of cross-ply laminated composite beams with general boundary conditions. Compos Sci Technol 2007;67:1096–104.
[21] Kiani Y, Eslami MR. Thermal buckling analysis of functionally graded material beams. Int J Mech Mater Des 2010;6:229–38.
[22] Shahba A, Attarnejad R, Marvi MT, Hajilar S. Free vibration and stability analysis of axially functionally graded tapered Timoshenko beams with classical and non-classical boundary conditions. Compos B 2011;42:801–8.
[23] Nateghi A, Salamat-talab M, Rezapour J, Daneshian B. Size dependent buckling analysis of functionally graded micro beams based on modified couple stress theory. Appl Math Model 2012;36:4971–87.
[24] Akgöz B, Civalek Ö. Buckling analysis of functionally graded microbeams based on the strain gradient theory. Acta Mech 2013;224:2185–201.
[25] Aydogdu M. Semi-inverse method for vibration and buckling of axially functionally graded beams. J Reinforced Plast Compos 2008;27:683–91.
[26] Huang Y, Li XF. Buckling analysis of nonuniform and axially graded columns with varying flexural rigidity. J Eng Mech 2011;137(1):73–81.
[27] Li XF, Wang BL, Han JC. A higher-order theory for static and dynamic analyses of functionally graded beams. Arch Appl Mech 2010;80:1197–212.
[28] Vo TP, Thai HT, Nguyen TK, Inam F, Lee J. Static behaviour of functionally graded sandwich beams using a quasi-3D theory. Compos Part B 2015;68:59–74.
[29] Filippi M, Carrera E, Zenkour AM. Static analyses of FGM beams by various theories and finite elements. Compos B 2015;72:1–9.
[30] Giunta G, Belouettar S, Carrera E. Analysis of FGM beams by means of classical and advanced theories. Mech Adv Mater Struct 2010;17:622–35.
[31] Mashat DS, Carrera E, Zenkour AM, Khateeb SAA, Filippi M. Free vibration of FGM layered beams by various theories and finite elements. Compos B 2014;59:269–78.
[32] Vo TP, Thai H-T, Nguyen T-K, Inam F, Lee J. A quasi-3D theory for vibration and buckling of functionally graded sandwich beams. Compos Struct 2015;119:1–12.
[33] Mantari JL, Yarasca J. A simple and accurate generalized shear deformation theory for beams. Compos Struct 2015;134:593–601.
[34] Mantari JL. A refined theory with stretching effect for the dynamics analysis of advanced composites on elastic foundation. Mech Mater 2015;86:31–43.
[35] Mantari JL. Refined and generalized hybrid type quasi-3D shear deformation theory for the bending analysis of functionally graded shells. Compos B 2015;83:142–52.
[36] Nguyen TK, Vo TP, Nguyen BD, Lee J. An analytical solution for buckling and vibration analysis of functionally graded sandwich beams using a quasi-3D shear deformation theory. Compos Struct 2016;156:238–52.
[37] Nemat-Alla M. Reduction of thermal stresses by developing two-dimensional functionally graded materials. Int J Solids Struct 2003;40:7339–56.
[38] Goupee AJ, Vel SS. Optimization of natural frequencies of bidirectional functionally graded beams. Struct Multidisc Optim 2006;32:473–84.
[39] Lü CF, Chen WQ, Xu RQ, Lim CW. Semi-analytical elasticity solutions for bidirectional functionally graded beams. Int J Solids Struct 2008;45:258–75.
[40] Zhao L, Chen WQ, Lü CF. Symplectic elasticity for two-directional functionally graded materials. Mech Mater 2012;54:32–42.
[41] Simsek M. Buckling of Timoshenko beams composed of two-dimensional functionally graded material (2D-FGM) having different boundary conditions. Compos Struct 2016;149:304–14.
[42] Karamanli A. Elastostatic analysis of two-directional functionally graded beams using various beam theories and Symmetric Smoothed Particle Hydrodynamics method. Compos Struct 2017;160:653–69.
[43] Pydah A, Sabale A. Static analysis of bi-directional functionally graded curved beams. Compos Struct 2017;160:867–76.
[44] Donning BM, Liu WK. Meshless methods for shear-deformable beams and plates. Comput Methods Appl Mech Eng 1998;152:47–71.
[45] Gu YT, Liu GR. A local point interpolation method for static and dynamic analysis of thin beams. Comput Methods Appl Mech Eng 2001;190(42):5515–28.
[46] Ferreira AJM, Roque CMC, Martins PALS. Radial basis functions and higher-order shear deformation theories in the analysis of laminated composite beams and plates. Compos Struct 2004;66:287–93.

[47] Ferreira AJM, Fasshauer GE. Computation of natural frequencies of shear deformable beams and plates by an RBF-pseudospectral method. Comput Methods Appl Mech Eng 2006;196:134–46.
[48] Moosavi MR, Delfanian F, Khelil A. The orthogonal meshless finite volume method for solving Euler-Bernoulli beam and thin plate problems. Finite Elem Anal Des 2011;49:923–32.
[49] Wu CP, Yang SW, Wang YM, Hu HT. A meshless collocation method for the plane problems of functionally graded material beams and plates using the DRK interpolation. Mech Res Commun 2011;38:471–6.
[50] Roque CMC, Figaldo DS, Ferreira AJM, Reddy JN. A study of a microstructure-dependent composite laminated Timoshenko beam using a modified couple stress theory and a meshless method. Compos Struct 2013;96:532–7.
[51] Qian LF, Batra RC. Design of bidirectional functionally graded plate for optimal natural frequencies. J Sound Vib 2005;280:415–24.
[52] Pilafkan R, Folkow PD, Darvizeh M, Darvizeh A. Three dimensional frequency analysis of bidirectional functionally graded thick cylindrical shells using a radial point interpolation method (RPIM). Eur J Mech A/Solids 2013;39:26–34.
[53] Yang Y, Kou KP, Lu VP, Lam CC, Zhang CH. Free vibration analysis of two-dimensional functionally graded structures by a meshfree boundary–domain integral equation method. Compos Struct 2014;110:342–53.
[54] Zhang GM, Batra RC. Symmetric smoothed particle hydrodynamics (SSPH) method and its application to elastic problems. Comput Mech 2009;43:321–40.
[55] Batra RC, Zhang GM. SSPH basis functions for meshless methods, and comparison of solutions with strong and weak formulations. Comput Mech 2008;41:527–45.
[56] Tsai CL, Guan YL, Batra RC, Ohanehi DC, Dillard JG, Nicoli E, et al. Comparison of the performance of SSPH and MLS basis functions for two-dimensional linear elastostatics problems including quasistatic crack propagation. Comput Mech 2013;51:19–34.
[57] Tsai CL, Guan YL, Ohanehi DC, Dillard JG, Dillard DA, Batra RC. Analysis of cohesive failure in adhesively bonded joints with the SSPH meshless method. Int J Adhes Adhes 2014;51:67–80.
[58] Wong SM, Hon YC, Golberg MA. Compactly supported radial basis functions for shallow water equations. Appl Math Comput 2002;127:79–101.